10. Lee, J. L., and R. S. Brodkey, *A.I.Ch.E. J.*, **10**, 187 (1964).
11. Rosensweig, R. E., Sc.D. thesis, Massachusetts Inst. Technol., Cambridge (1959).
12. ———, H. C. Hottel, and G. C. Williams, *Chem. Eng. Sci.*, **15**, 111 (1961).
13. Becker, H. A., Sc.D. thesis, Massachusetts Inst. Technol., Cambridge (1961).
14. ———, H. C. Hottel, and G. C. Williams, paper presented at Ninth Symp. (International) on Combustion (1962).
15. ————————, paper presented at A.I.Ch.E. Houston meeting (Dec., 1963).
16. Baldwin, L. V., and T. J. Walsh, *A.I.Ch.E. J.*, 7, 53 (1961).
17. Flint, D. I., Hisao Kada, and T. J. Hanratty, *ibid.*, **6**, 325 (1960).
18. Mickelson, W. R., *Natl. Advisory Committee Aeronaut. Tech. Note 3570* (1955).
19. Towle, W. L., and T. K. Sherwood, *Ind. Eng. Chem.*, **31**, 457 (1939).
20. Batchelor, G. K., *J. Fluid Mech.*, **5**, 113 (1959).
21. Forslund, R. P., and H. B. Sargent, "Influence of Reynolds Number on Mixing in Turbulent Free Jets," Linde Speedway Res. Lab., Indianapolis, Ind. (1961).
22. Wilson, R. A. M., and P. V. Danckwerts, *Chem. Eng. Sci.*, **19**, 885 (1964).

Manuscript received December 9, 1965; revision received March 21, 1966; paper accepted March 30, 1966. Paper presented at A.I.Ch.E. Boston meeting.

Hydrodynamics of Rivulet Flow

G. D. TOWELL and L. B. ROTHFELD

Shell Development Company, Emeryville, California

A theoretical analysis of the hydrodynamics of liquid rivulets flowing down an inclined surface is presented. Steady state solutions are developed for the laminar flow case which relate the flow rate to the rivulet width, the physical properties of the liquid, and the contact angle. Excellent verification of the theoretical predictions was obtained in a number of experiments with various liquids on an inclined glass plate. All constants in the equations were derived from theory. These results will be useful in obtaining a better understanding and correlation of such phenomena as liquid flow over packings and catalysts and flow along walls and tube surfaces, as in condensation and evaporation.

When a liquid flows down an inclined surface at a low rate, separate rivulets form instead of a continuous film. This is an important phenomenon in the operation of packed contactors where packings are used to distribute the liquid; trickle phase reactors where the liquid is distributed over a catalyst; and in condensation and evaporation on surfaces.

The objective of this work is to study theoretically and experimentally the hydrodynamics of rivulet flow on an inclined flat surface. (The contiguous gas phase is stationary.) Steady state theoretical solutions are developed for the laminar flow situation which is a realistic one over a wide range of rivulet flow rates. A reduced form of the Navier-Stokes equations is solved with special boundary conditions of a finite contact angle at the edge of the rivulet and relations between the pressure inside and outside a curved interface. The shape of the interface and the velocity profile in the rivulet are obtained, and an integration of this velocity profile gives a relation between the rivulet width and the flow rate. This relation contains the plate inclination; the contact angle of the liquid on the plate; and the fluid properties, viscosity, density, and surface tension.

Experiments were carried out over a wide range of flow rates with a variety of liquids on a glass plate at different inclinations. Measurements of rivulet width as a function of flow rate were made in the region where the rivulet had attained steady state. Optical measurements were made of the contact angle on the edge of the actual moving rivulet. The experimental values of the rivulet width were compared with theoretical values computed from the measured flow rate and contact angle. Above a certain flow rate waves appeared on the film and observations were made of the incidence and character of these waves.

THEORY

Development of Flow and Interface Equations

The problem of describing theoretically the flow of a rivulet entails two aspects: the description of the gas-liquid interface and the calculation of the velocity distribution. The theory developed below considers only that portion of the stream which has traveled far enough so that the shape of the cross section no longer changes along the stream path. The flow is then considered to be one dimensional, with a velocity component only in the direction of the stream. Since acceleration effects are neglected, the equations of motion (Navier-Stokes equations) sim-

L. B. Rothfeld is with Shell Oil Company, Deer Park, Texas.

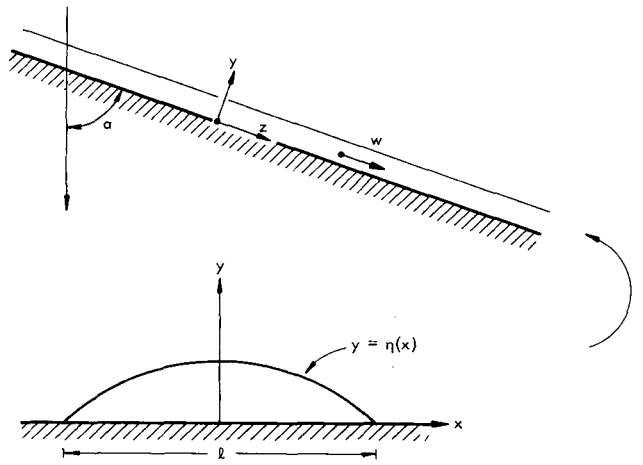

Fig. 1. Coordinate axes.

plify to a balance of viscous and gravitational forces. The problem of calculating the shape of the interface resembles that of calculating the shape of a meniscus under the influence of surface tension and gravity, except that here the interface is two dimensional. Once the shape of the interface and the velocity distribution are known, the flow rate for a stream of given width can be calculated. The results are expressed in terms of a dimensionless flow group which depends on a dimensionless stream width and the contact angle.

Consider the flow of a rivulet down an inclined flat surface, as shown in Figure 1, with the following assumptions:

1. One-dimensional flow parallel to z axis ($u = v = 0$)
2. Fully developed flow, that is, the stream is of uniform width and derivatives with respect to z are zero.
3. Steady state.
4. The liquid is incompressible.
5. No shear at the gas-liquid interface.

With these assumptions, the Navier-Stokes equations reduce to the following:

$$\frac{\partial p}{\partial x} = 0 \tag{1}$$

$$\frac{\partial p}{\partial y} = -\rho g \sin \alpha \tag{2}$$

$$\frac{\partial^2 w}{\partial x^2} + \frac{\partial^2 w}{\partial y^2} = -\frac{g \cos \alpha}{\nu} \tag{3}$$

Two boundary conditions follow from the absence of slip and from symmetry:

$$w = 0 \text{ at } y = 0 \tag{4}$$

$$\frac{\partial w}{\partial x} = 0 \text{ at } x = 0 \tag{5}$$

At the gas-liquid interface, given by $y = \eta(x)$, the z component of the shear stress must be zero. Therefore

$$\tau_{yz}|dx| + \tau_{xz}|dy| = 0$$

and if

$$\eta' = \frac{d\eta}{dx}$$

In order to solve Equation (3) subject to conditions (4) to (6), an equation for the interface $\eta(x)$ must be developed. For this purpose, the starting point is the well-known expression for curved interfaces:

$$\lim_{y \to \eta^-} (\tau_n) - \lim_{y \to \eta^+} (\tau_n) = \gamma \left[-\frac{\eta''}{(1 + \eta'^2)^{3/2}} \right]$$

where

$$\eta'' = \frac{d^2\eta}{dx^2}$$

and the expression in brackets is the reciprocal of the radius of curvature. By use of Equation (6), it can be shown that the normal stress is identically equal to the pressure. Thus

$$p(\eta) = p_g - \frac{\gamma \eta''}{(1 + \eta'^2)^{3/2}} \tag{7}$$

where

$$p(\eta) = \lim_{y \to \eta^-} (p)$$

By Equation (1) the pressure in the liquid is independent of x. Integration of Equation (2) leads to

$$p(\eta) = C_1 - \rho g \eta \sin \alpha \tag{8}$$

where C_1 is an integration constant. By elimination of $p(\eta)$ between (7) and (8), and with use of a change of variables

$$\frac{Y''}{(1 + Y'^2)^{3/2}} = \frac{a}{b} + Y \tag{9}$$

where $Y = (\eta_o - \eta)/a$ and the primes denote differentiation with respect to $X = x/a$. The coordinate system has been rotated 180 deg. and shifted so that its origin is at the uppermost point on the rivulet (Figure 2), and linear dimensions have been scaled relative to the capillary constant

$$a = \sqrt{\gamma/\rho g \sin \alpha}$$

All constants have been combined to form a new constant b. By inspection of Equation (9), b is seen to be the radius of curvature at $Y = 0$.

The solution of Equation (9) consists of a family of curves of Y vs. X with a/b as parameter. For a given contact angle and stream width, one of these curves describes the liquid-gas interface. The constant a/b cannot be chosen arbitrarily, as it is uniquely determined by the choice of stream width and contact angle.

The problem of calculating the flow rate for a given stream width and contact angle entails the following. To find the shape of the interface, Equation (9) is solved subject to the boundary conditions:

$$Y = 0 \text{ at } X = 0 \tag{10}$$

$$Y' = 0 \text{ at } X = 0 \tag{11}$$

Solution of Equation (3) with boundary conditions (4) to (6) provides the velocity distribution $w(x, y)$. Then

$$Q = \int_{-l/2}^{l/2} \int_0^{\eta} w(x, y)\, dy dx \tag{12}$$

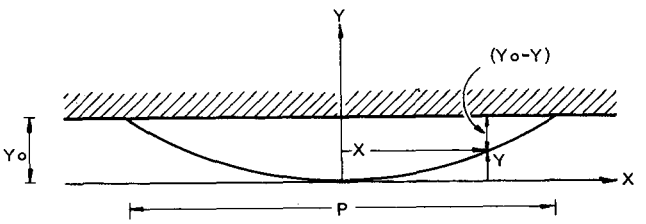

Fig. 2. Coordinate axes.

In dimensionless form, Equations (3), (4), (5), (6), and (12) are

$$\frac{\partial^2\omega}{\partial X^2} + \frac{\partial^2\omega}{\partial \xi^2} + 1 = 0 \tag{13}$$

$$\omega = 0 \text{ at } \xi = 0 \tag{14}$$

$$\frac{\partial\omega}{\partial X} = 0 \text{ at } X = 0 \tag{15}$$

$$|Y'|\frac{\partial\omega}{\partial X} + \frac{\partial\omega}{\partial \xi} = 0 \text{ at } \xi = \eta_0/a - Y \tag{16}$$

$$\Omega = \int_{-P/2}^{P/2}\int_{0}^{(Y_0-Y)} \omega(X,\xi)\,d\xi\,dX \tag{17}$$

where

$$X = x/a,\ \xi = y/a,\ P = l/a = \frac{l}{\sqrt{\gamma/\rho g \sin\alpha}}$$

$$\omega = \frac{\mu w \tan\alpha}{\gamma},\ Y_o = \eta_0/a$$

$$\Omega = \frac{\mu\rho g Q}{\gamma^2}\tan\alpha\sin\alpha$$

The dimensionless flow rate Ω is then a function of the dimensionless stream width P as shown by Equation (17), and of the contact angle θ.

Simplification and Integration of Flow Equation

In general the equation which describes the shape of the interface will be too complex to permit an analytical solution of Equation (13). An approximate solution can be obtained easily by assuming that

$$\frac{\partial^2\omega}{\partial X^2} << \frac{\partial^2\omega}{\partial \xi^2}$$

and by taking

$$\frac{\partial\omega}{\partial\xi} = 0 \text{ at } \xi = \eta_0/a - Y \tag{18}$$

as the boundary condition at the liquid-gas interface. These assumptions are justified when the rivulet is relatively flat, that is, when the contact angle is small. To develop a more exact solution suitable for larger contact angles, the approximate solution can be used as a starting point for a perturbation solution of Equation (13).

Only the approximate solution will be given here. With the above assumptions, Equation (13) becomes

$$\frac{d^2\omega}{d\xi^2} + 1 = 0$$

The solution, subject to boundary conditions (14) and (18), is

$$\omega = (Y_o - Y)\,\xi - \frac{1}{2}\xi^2 \tag{19}$$

The velocity profile is parabolic, as expected for a one-dimensional flow influenced only by viscous and gravity forces. By substitution of Equation (19) into (17) and integration with respect to ξ, we obtain

$$\Omega = \frac{2}{3}\int_0^{P/2} -(Y_o - Y)^3\,dX \tag{20}$$

We now proceed to a solution of the interface equation for substitution in Equation (20). Equation (9) is the two-dimensional version of the equation for the shape of a meniscus. Rayleigh (5, 6) solved the equation for the limiting case of a large radius of curvature ($a/b \to 0$),

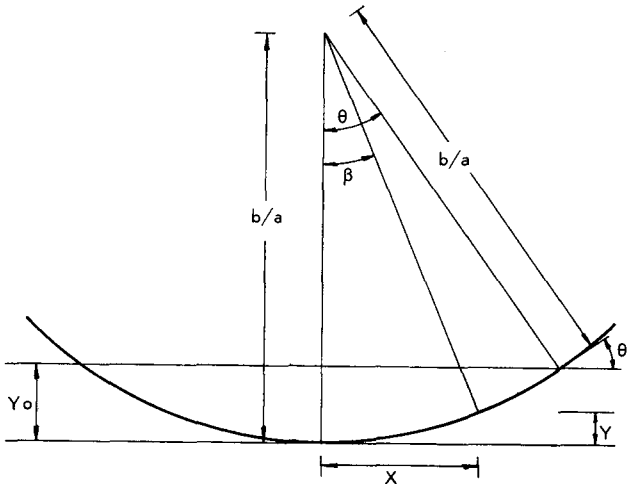

Fig. 3. Geometry of sector shape rivulet.

and Goodrich (1) has recently published a general solution without derivation. Because the derivation provides physical insight, it will be outlined below.

Solutions for Limiting Case of Small Rivulet

When the radius of curvature is small, $a/b >> Y$, and Equation (9) becomes

$$\frac{Y''}{(1+Y'^2)^{3/2}} = \frac{a}{b} = \delta \tag{21}$$

which is the equation of a circle of radius b/a. In this limit, the rivulet is so shallow and narrow that its shape is governed only by surface tension, and the influence of gravity on the shape is negligible. The cross section of the stream is a sector of a circle, with its chord length equal to the width. The radius is such that Y' at the chord is the tangent of the contact angle.

Although the equation of the interface can be derived from Equation (21), it is simpler to calculate it by geometrical arguments. From Figure 3

$$Y_o - Y = (b/a)[\cos\beta - \cos\theta]$$

$$= \sqrt{(b/a)^2 - X^2} - (b/a)\cos\theta$$

$$b/a = \frac{P}{2\sin\theta}$$

substitution of these relations into Equation (20) leads to

$$\Omega = \frac{P^4}{24\sin^4\theta}\int_0^{\sin\theta}[\sqrt{1-(x/b)^2} - \cos\theta]^3\,d(x/b)$$

After carrying out the integration, the result is

$$\Omega = P^4\frac{f(\theta)}{192} \tag{22}$$

where

$$f(\theta) = \frac{12\theta\cos^2\theta + 3\theta - 2\cos^3\theta\sin\theta - 13\cos\theta\sin\theta}{\sin^4\theta} \tag{23}$$

Equation (22) may also be written as

$$\frac{\mu Q}{\rho l^4 g\cos\alpha} = \frac{f(\theta)}{192} \tag{24}$$

The curves in Figure 5 show that the stream width is extremely sensitive to contact angle and for a given contact angle, the stream width is proportional to the one-quarter power of the flow rate and the kinematic viscosity and

inversely proportional to the one-quarter power of the density. Curiously, the stream width is independent of the surface tension.

For values of θ less than about 15 deg., Equation (23) is not suitable for numerical calculations. When θ is small, the following equation is useful:

$$f(\theta) = \frac{(204/315)\ \theta^3 + 0(\theta^5)}{1 - (2/3)\ \theta^2 + 0(\theta^4)} \tag{25}$$

Equation (25) was derived from Equation (23) by expanding the trigonometric functions in Maclaurin series and dropping terms of order higher than θ^7.

Solution for Limiting Case of Wide Flat Rivulet

As the flow rate increases, the rivulet widens and deepens, maintaining for a while its circular interface. Eventually the stream becomes deep enough so that the influence of gravity on the shape of the interface can no longer be neglected. Both terms on the right-hand side of Equation (9) must be retained when solving for the shape of the interface. Finally, the stream becomes wide enough and flat enough so that

$$a/b << Y$$

In this limiting case, Rayleigh's solution (5) shows that the stream reaches a maximum depth given by

$$Y_o = 2 \sin (\theta/2)$$

As the flow rate increases, the stream widens but no longer deepens. In this region, the flow rate may be calculated by assuming that the stream cross section is rectangular with depth 2 sin $(\theta/2)$ and width P. Equation (20) becomes

$$\Omega = \frac{2}{3} \int_0^{P/2} Y_o^3 dx = \frac{1}{3} Y_o^3 P$$

or

$$\Omega = \frac{8}{3} P \sin^3 (\theta/2) \tag{26}$$

Equation (26) may also be written

$$\frac{\mu Q \tan \alpha}{l\gamma} \sqrt{\frac{\rho g \sin \alpha}{\gamma}} = \frac{8}{3} \sin^3 (\theta/2) \tag{27}$$

Once again the rivulet width is seen to be very sensitive to contact angle (see Figure 5). The width is now a strong function of surface tension ($\propto \gamma^{-1.5}$) and is proportional to the viscosity and flow rate and (density)$^{0.5}$.

General Solutions

In the intermediate region where the interface is neither flat nor circular, Equation (9) may be integrated once by noting that

$$Y'' = Y' \frac{dY'}{dY}$$

so that

$$\frac{Y' dY'}{(1 + Y'^2)^{3/2}} = (\delta + Y) dY$$

where

$$\delta = a/b$$

After integrating and noting that from Equations (10) and (11)

$$Y' = 0 \text{ at } Y = 0$$

the result is

$$\frac{1}{\sqrt{1 + Y'^2}} = 1 - \delta Y - \frac{1}{2} Y^2 \tag{28}$$

The maximum depth Y_o can be obtained from Equation (28) by setting

$$|Y'| = \tan \theta \text{ at } Y = Y_o$$

Then

$$\frac{1}{2} Y_o^2 + \delta Y = 1 - \frac{1}{\sqrt{1 + \tan^2 \theta}} = 1 - \cos \theta$$

so that

$$Y_o = -\delta + \sqrt{\delta^2 + 2(1 - \cos \theta)} \tag{29}$$

Note that

$$\lim_{\delta \to 0} (Y_o) = 2 \sin (\theta/2)$$

in agreement with Rayleigh's equation.

The solution of Equation (28) is simplified by introducing the change of variables

$$Z = Y + \delta$$

Then Equation (28) becomes

$$\frac{1}{\sqrt{1 + Z'^2}} = 1 + \frac{1}{2} \delta^2 - \frac{1}{2} Z^2 \tag{30}$$

with boundary condition

$$Z = \delta \text{ at } X = 0 \tag{31}$$

When Equation (30) is solved for Z'

$$Z' = \frac{\sqrt{-1/4[Z^2 - (4 + \delta^2)][Z^2 - \delta^2]}}{1 + 1/2\ \delta^2 - 1/2\ Z^2}$$

After separating variables and integrating, with use of boundary condition (31), we obtain

$$X = \frac{1}{\sqrt{4 + \delta^2}} \int_1^u \frac{(1 + \delta^2) + (1 - \delta^2 u^2)}{\sqrt{(u^2 - 1)(1 - c^2 u^2)}} du$$

where

$$u = Z/\delta$$

and

$$c^2 = \frac{\delta^2}{4 + \delta^2}$$

The above integral is an elliptic integral, which can be reduced to standard forms by methods described by Karman and Biot (2). The result is

$$X = \frac{2 - k^2}{k} [K - F(k, \phi)] - \frac{2}{k} [E - E(k, \phi] \tag{32}$$

where $F(k, \phi)$ and $E(k, \phi)$ are defined as

$$F(k, \phi) = \int_0^{\phi} \frac{d\phi}{\sqrt{1 - k^2 \sin^2 \phi}}$$

$$E(k, \phi) = \int_0^{\phi} \sqrt{1 - k^2 \sin^2 \phi}\ d\phi$$

and K and E are defined as

$$K = F(k, \pi/2)$$

$$E = E(k, \pi/2)$$

Also

$$k = \frac{2}{\sqrt{4 + \delta^2}} \tag{33}$$

$$Z = \frac{2}{k} \sqrt{1 - k^2 \sin^2 \phi} \tag{34}$$

Equations (32) and (34) are identical to those given by Goodrich (1); his α is $\sin^{-1} k$.

The shape of the interface is given implicitly by Equations (32) and (34) in terms of the parameter ϕ. This parameter decreases from $\pi/2$ at $X = 0$ to a minimum value ϕ_{min} at the outer edge of the rivulet. As ϕ decreases from $\pi/2$ to ϕ_{min}, Z increases from δ to Z_{max}, and from Equation (34)

$$Z_{max} = \frac{2}{k}\sqrt{1 - k^2 \sin \phi_{min}} \tag{35}$$

Also, from Equation (30) with $|Z'| = \tan \theta$

$$Z^2_{max} = \delta^2 + 4 \sin^2 (\theta/2) \tag{36}$$

by elimination of Z_{max} between Equations (35) and (36),

$$\sin \phi_{min} = \cos (\theta/2) \tag{37}$$

Then from Equation (32)

$$\frac{P}{2} = \frac{2 - k^2}{k}[K - F(k, \phi_{min})] - \frac{2}{k}[E - E(k, \phi_{min})] \tag{38}$$

In order to calculate Ω for given P and θ, it is necessary to find the shape of the interface (Z vs. X) and to evaluate the integral in Equation (20). Numerical integration requires values of Y at specified values of X. In principle, one can find k from Equations (37) and (38) and then use Equation (32) to obtain values of ϕ corresponding to the specified values of X. These values of ϕ could then be substituted into Equation (34) to obtain the value of Z and thus Y. However, the equations are such that it is difficult to devise convergent iteration procedures for the trial and error solutions. Therefore the following procedure has been adopted.

Values of θ and δ rather than θ and P are taken as starting point. Then P is calculated from Equations (33), (37), and (38). For each of a series of values of ϕ between $\pi/2$ and ϕ_{min}, values of Z and X are calculated by use of Equations (32) and (34). The flow rate is computed from Equation (20) by the use of a Legendre-Gauss integration formula, which requires values of Y at five specified X. These are obtained from the above set of Z vs. X by means of a five-point, divided-difference interpolation formula. An IBM 7090 Fortran program has been written to perform the calculations.

Numerical Results

The numerical results are given in Table 1 in the form of P and Ω values at specified values of θ. Figure 4 shows some numerical results for the shape of the interface; one case is a wide flat rivulet and the other a narrow circular segment shape. The results in Table 1 are presented graphically in Figure 5 in which the rivulet width group P is plotted vs. the rivulet flow group Ω with the contact angle θ as a parameter. The points shown are the actual numerical computations. The dashed lines in Figure 5 are the asymptotic solutions for wide flat rivulets at high Ω values [Equation (26)] and for narrow rivulets at low Ω values [Equation (22)]. The asymptotic solutions for narrow rivulets agree quite closely with the numerical solutions at P values less than 4, which encompasses a large amount of the total region. The asymptotic solution for wide rivulets is a good approximation at P values greater than 20. If the two asymptotic solutions were extrapolated to their intersection, a reasonable estimate of the correct solution would still be obtained; the maximum error on P at a given Ω would then be about +60%.

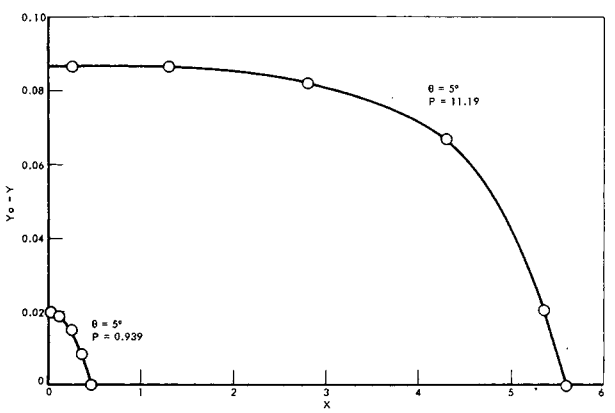

Fig. 4. Shape of interface; numerical results.

Table 1. Numerical Results

θ Deg.	θ Rad.	δ	P	Ω
0.5	0.008727	0.0005	6.60	6.4×10^{-7}
		0.001	5.53	4.4×10^{-7}
1.0	0.01745	0.0001	8.83	9.04×10^{-6}
		0.0005	7.98	7.6×10^{-6}
		0.001	6.91	5.8×10^{-6}
		0.01	2.65	4.3×10^{-7}
2.0	0.0349	0.0001	10.2	9.20×10^{-5}
		0.0005	9.37	8.02×10^{-5}
		0.001	8.29	6.56×10^{-5}
		0.01	3.93	1.20×10^{-5}
		0.04	1.58	5.4×10^{-7}
		0.07	0.96	0.7×10^{-7}
3.0	0.05236	0.0001	11.02	3.50×10^{-4}
		0.0005	10.18	3.10×10^{-4}
		0.001	9.10	2.60×10^{-4}
		0.01	4.71	6.64×10^{-5}
		0.04	2.17	5.91×10^{-6}
		0.07	1.38	1.13×10^{-6}
		0.10	1.004	3.3×10^{-7}
4	0.0698	0.0001	11.60	8.96×10^{-4}
		0.0005	10.75	8.01×10^{-4}
		0.001	9.68	6.81×10^{-4}
		0.01	5.28	2.09×10^{-4}
		0.04	2.65	2.79×10^{-5}
		0.07	1.76	6.57×10^{-6}
		0.1	1.30	2.12×10^{-6}
		0.179	0.761	2.6×10^{-7}
5	0.0873	0.0001	12.04	1.85×10^{-3}
		0.0005	11.19	1.67×10^{-3}
		0.001	10.12	1.43×10^{-3}
		0.01	5.72	4.91×10^{-4}
		0.04	3.04	8.63×10^{-5}
		0.07	2.09	2.40×10^{-5}
		0.1	1.575	8.54×10^{-6}
		0.179	0.939	1.17×10^{-6}
10	0.1745	0.0005	12.57	1.58×10^{-2}
		0.001	11.50	1.38×10^{-2}
		0.01	7.09	5.98×10^{-3}
		0.04	4.34	1.99×10^{-3}
		0.07	3.28	8.77×10^{-4}
		0.10	2.64	4.34×10^{-4}
		0.179	1.72	9.53×10^{-5}
		1.0	0.346	1.8×10^{-7}
20	0.349	0.0005	13.92	1.44×10^{-1}
		0.001	12.84	1.29×10^{-1}
		0.01	8.44	6.72×10^{-2}
		0.04	5.67	3.02×10^{-2}
		0.07	4.57	1.82×10^{-2}
		0.10	3.88	1.17×10^{-2}
		0.179	2.80	4.30×10^{-3}
		1	0.671	2.08×10^{-5}

EXPERIMENTAL PROGRAM

Experimental measurements, consisting basically of rivulet width measurements as a function of liquid flow rate, were conducted to test the theory. An inclined glass plate was used in all experiments and a variety of liquids was used in order to vary the physical properties. Contact angles were measured on the edge of the moving rivulet by an optical technique.

The experimental apparatus is illustrated schematically in Figure 6. The glass plate was 120 cm. long and 60 cm. wide and was mounted in a wooden frame which had a Plexiglas lid to keep dust particles off the plate. The plate angle could be varied by a pulley and sliding track arrangement on a rigid metal frame attached to the floor. The liquid was circulated over the plate by pumps from a liquid sump mounted at the bottom of the plate. Three separate stainless steel liquid loops were installed so that three rivulets could be examined at the same time. One of the loops contained a small centrifugal pump which supplied the highest flow rate, which ranged from 30 to 200 ml./min. Flow control in this loop was by manual control valve and rotameter. The intermediate flow range from 1 to 60 ml./min. was supplied by a positive displacement pump (a Whitey microregulating laboratory feed pump). The flow control in this intermediate loop was achieved by changing the stroke of the pump and the flow was measured by a rotameter. The low flow range from 0.03 to 5 ml./min. was supplied by a second positive displacement pump (a Milton Roy mini pump) also with variable stroke flow control. The flow in the lowest range was measured by rate of fall in a burette attached to the pump suction. Small air reservoirs were attached to the outlet of both of the positive displacement pumps to remove slight flow surges. The width of the rivulets was obtained from strips of graph paper glued to the underside of the glass plate. The intermediate and low flow rate rivulets were introduced onto the plate by stainless steel tubing almost touching and at right angles to the plate. The high flow rate streams were introduced onto the plate with a header containing a number of holes; this prevented the excessive jetting that occurred with a straight tube inlet.

The plate cleaning method was simple and consisted of washing with an industrial cleaner (containing detergent, bleach, and a mild abrasive) followed by rinsing with distilled water and ending up with squeegee removal of excess water. No particular effort was made to obtain a scrupulously clean surface; the washing was mainly used to remove dust and dirt particles from the plate.

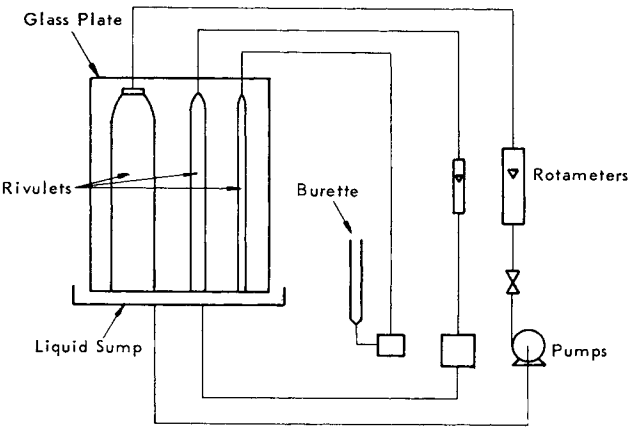

Fig. 6. Schematic of apparatus.

The contact angle of the liquid with the glass surface was measured by a simple method developed by Langmuir (*4*) and illustrated in Figure 7. The method consists basically of locating the normal to the plate and to the liquid at the edge of the rivulet. The normals are easily located by viewing the reflection of a point light source through a slit where the light source is close to the slit. The slit and light source device traveled along a scale, mounted a known distance above and parallel to the plate surface. The normals were accurately located by moving the slit to the position where the reflection of the light just disappears. The contact angle is then simply related to the distance between the two slit positions and the distance of the slit above the plate. This technique was precise enough to obtain contact angles to within ½ deg.

The experimental procedure consisted of flowing the rivulets over the plate at a constant flow rate until the rivulet width obtained a steady state value. Measurements were then made of the rivulet width at a number of positions down the plate. The contact angle was then measured on both sides of the moving rivulet at a number of positions down the plate. These measurements, together with the flow rate, constituted one set of data.

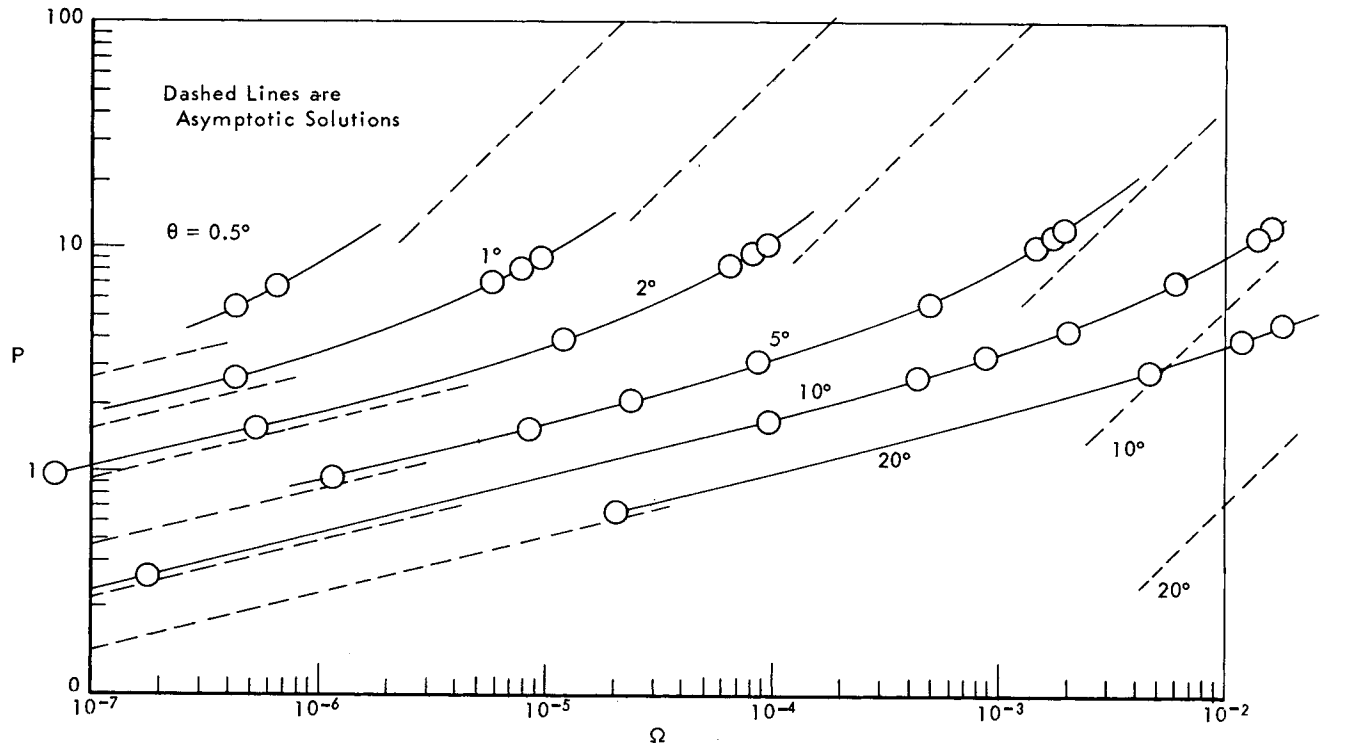

Fig. 5. Numerical results.

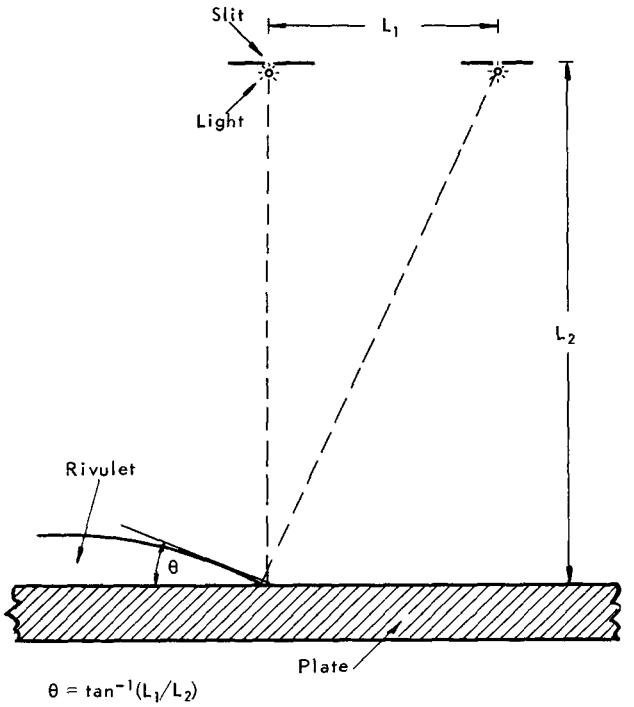

Fig. 7. Contact angle measurement.

EXPERIMENTAL RESULTS

Data for Water

The first data obtained were with tap water on a plate slope of 45 deg. The rivulet width was measured at a number of positions down the plate and an average width was taken over the region of constant width. This is a measure of the equilibrium width and is the width used in the theoretical derivations. The contact angle was similarly averaged over the region of constant width. A photograph of a water rivulet is shown in Figure 8. These average measured contact angles, measured stream widths, and the corresponding measured flow rates are contained in the first three columns of Table 2. The fourth column contains a theoretical value of the rivulet width based on the measured flow rate and contact angle and deduced from the theoretical curves in Figure 5. In using Figure 5, Ω was calculated from the measured flow rate (Ω includes the viscosity, density, and surface tension of the liquid as well as the plate inclination) and the corresponding P value found by interpolating for the measured contact angle. The theoretical rivulet width was then calculated from the P value (P includes liquid surface tension and density and plate inclination). Flow rates above 10 ml./min. resulted in a rippling flow regime, which is discussed in detail later on.

Table 2. Data for Water; Plate Angle 45 Deg.

Flow rate Q, ml./min.	Contact angle θ, deg.	Rivulet width l(exptl.), mm.	Rivulet width l(theory), mm.
0.033	4.5	2.5	2.9
0.20	8	3	3.0
0.43	3	6.5	7.8
1.14	4.5	7	7.2
6.2	9 to 12	7 to 8	5.5 to 6.8

Comparison of the measured and theoretical widths (last two columns in Table 2) shows that the theoretical

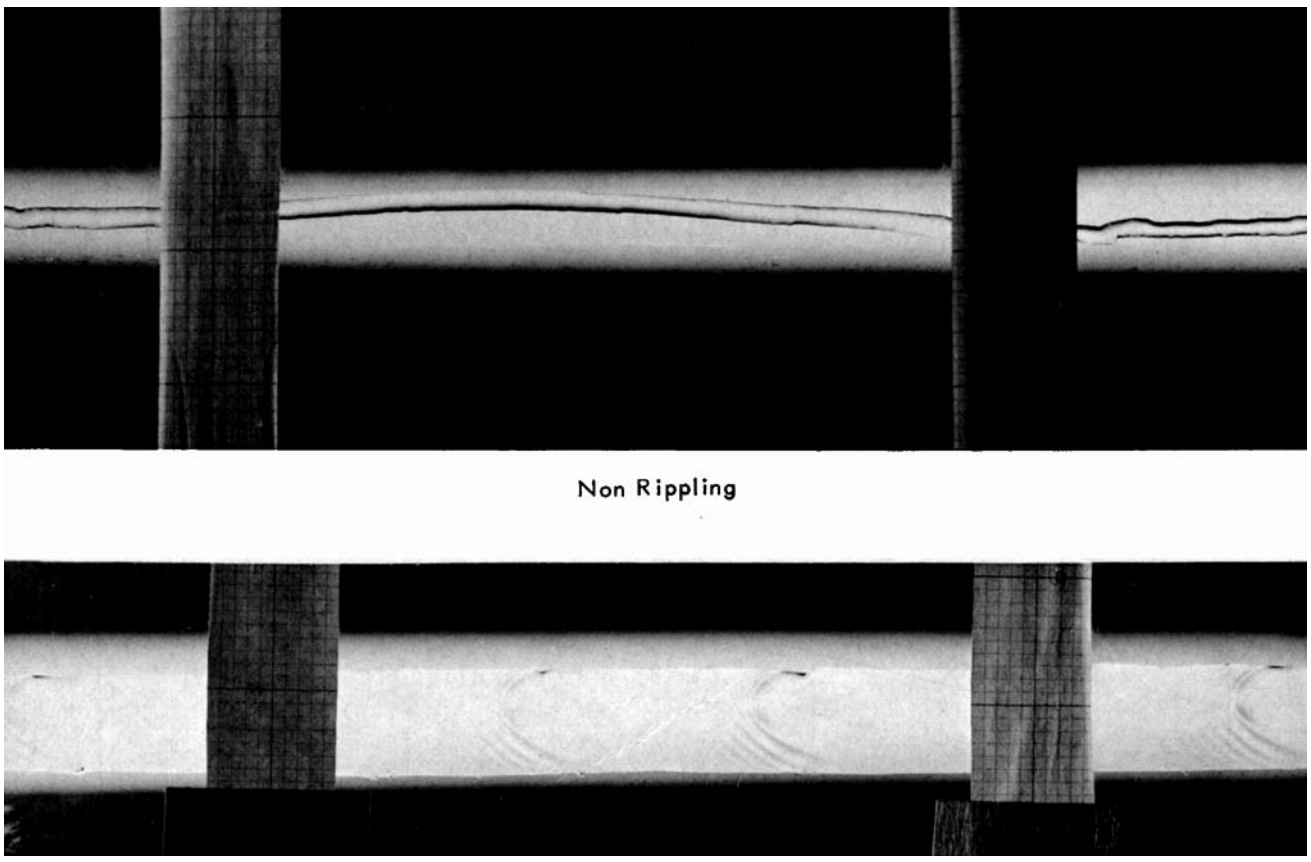

Fig. 8. Typical rivulets.

analysis is confirmed very well by the experiments. There was considerable variation in contact angle from run to run, due to differing surface conditions of the plate. As pointed out earlier no particular care was taken to get an absolutely clean surface, so this is not surprising. This does demonstrate the absolute necessity of measuring the contact angle in each individual run on the edge of the moving rivulet. Static measurements of contact angle on horizontal surfaces showed similar variations of contact angle.

Similar data were obtained for water at a plate angle of 80 deg. (almost flat plate) and the rivulets are wider compared with the 45-deg. slope (at the same flow and contact angle) as might be expected intuitively. Rippling did not occur in this case until the flow rate reached 36 ml./min. Once again the experimental widths agree quite well with the theoretical ones. Data were also obtained for a plate angle of 10 deg. (almost vertical plate), which also shows good agreement between theory and experiment. Rippling occurred on this plate at flows above 6 ml./min.

In order to test the theory at higher flow rates a surface active agent (Triton X-305) was added (at a concentration of 1.8 ml./liter) to suppress the rippling, permitting flow rates as high as 264 ml./min. without ripples on the 45-deg. plate. The surface tension was reduced to 40 dynes/cm. by this surfactant and this value was used in the calculation of the rivulet width from the theory.

The theoretical and measured widths are compared in Figure 9 for all the water runs that were free of ripples. The agreement is very good since most of the data fall within $\pm$ 20% of the theory. These data cover flow rates from 0.03 to 300 ml./min., plate angles of 10, 45, and 80 deg. and rivulet widths from 2 to 40 mm. This is equivalent to P values from 3 to 40 and Ω values from 10^{-7} to 10^{-2}, which from examination of Figure 5 shows that the complete range from one asymptotic solution to the other was covered. The discussions of the rippling flow data are given later in this report.

Effect of Viscosity and Surface Tension

Data were obtained with a 60% glycerol-water mixture to investigate the effect of viscosity (9.66 centipoise) The mixture has a density of 1.19 g./ml. and a surface tension 69.5 dynes/cm. The data and theory are compared in Figure 10, which shows that the theory adequately describes the effect of viscosity.

A hydrocarbon (n-dodecane) was used in a few experiments in order to test the effect of surface tension (25.5 dynes/cm.). These data and theory are also compared in Figure 10, which shows that surface tension effects are adequately described.

Effect of Contact Angle

Considerable variation in contact angle was obtained in all of the systems tested and since these data all fit the theory (Figures 9 and 10) this is confirmation that the theory does properly describe contact angle effects. A few additional experiments were made in which larger values of the contact angle were obtained (13 to 16 deg.) by running water over a plate that had been washed with n-dodecane. These data are also compared with theory in Figure 10 and confirm that the theory properly describes contact angle effects.

There was considerable variation in the values of the contact angle from one experiment to the next and this was undoubtedly due to surface contaminations. However since careful measurements of the contact angle were made in each experiment, proper account could be taken of these variations. Literature sources indicate that the liquids used in this work should completely wet a glass plate (presumably scrupulously cleaned). The contact angles obtained were indeed quite small in many cases, but as the analysis showed the actual value of the contact angle was a very sensitive parameter. We believe that experimentation with these apparently contaminated surfaces is quite proper since they are more like real surfaces that would occur in process equipment.

A few measurements of the static contact angle were made on a stationary drop of the liquids used and on the same glass plate. These values were similar to those measured on the edge of the moving stream. Some measurements were also made on the moving rivulet of the advancing and receding contact angle and as might be expected the advancing angle was always the higher. If a series of experiments is made with increasing flows, then the contact angle tends to increase and vice versa.

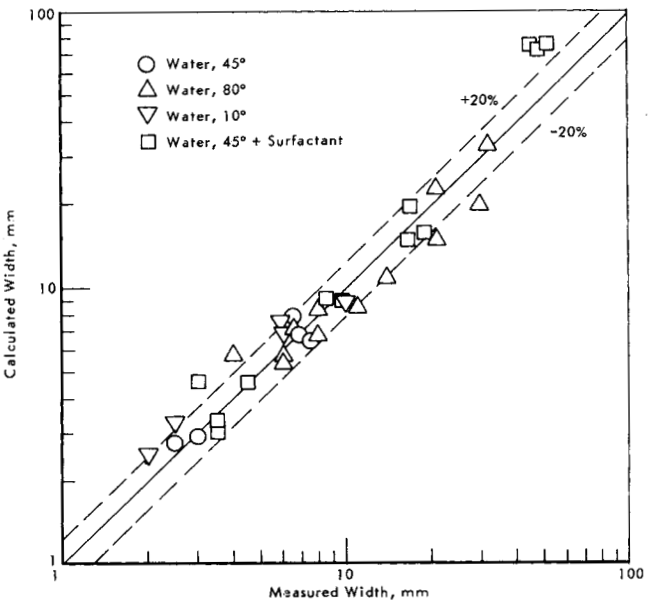

Fig. 9. Experimental vs. calculated width for water.

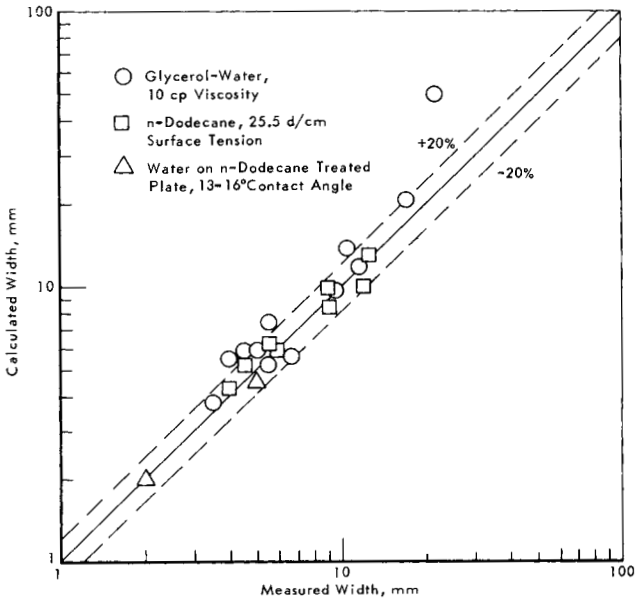

Fig. 10. Experimental vs. calculated width for gylcerol-water, n-dodecane, and water on oily plate.

TABLE 3. FLOW RATES FOR TRANSITION TO RIPPLING

	Flow rate, ml./min.	Rivulet width, mm.	N_{Re}
Water (10-deg. plate angle)	16 to 36	30 to 55	8.9 to 11
Water (45-deg. plate angle)	6.2 to 9.5	9.5 to 30	11 to 5.3
Water (80-deg. plate angle)	3.1 to 6.25	10 to 9.5	5.4 to 11
Glycerol-water	53 to 85	15 to 33	7.1 to 5.2
n-Dodecane	5.0	13	34

Rippling Flow

At flow rates above some critical value, ripples of a regular wavelength appear on the surface of the rivulets (Figure 8). All of the data presented are for ripple-free flows. Table 3 shows the transition flow rates for rippling. A range of flow rates in Table 3 indicates that no rippling occurs at the lower value and definite rippling at the upper value; hence the critical condition is somewhere in between. Critical Reynolds numbers were calculated (contained in Table 3) and were in the range of 5 to 10 which are similar to the critical values obtained in film flow. The Reynolds number is defined here as four times the flow rate per unit wetted periphery divided by the kinematic viscosity. By analogy with the film flow work of others, these waves on the rivulets are a laminar flow instability and not the onset of turbulence.

The theoretical development presented earlier does not include any representation of rippling, so that one would not expect prediction of rivulet widths with ripples present. The rivulet widths predicted from the nonrippling theory are usually less than the measured values in the rippling flow regime. As a very rough estimate, doubling of the theoretical prediction of the rivulet width suffices to represent the rippling flow stream width.

CONCLUSIONS

Equations have been developed which describe the hydrodynamics of laminar flow of a liquid rivulet down an inclined surface. Steady state solutions have been obtained for the case of no shear stress at the liquid gas boundary (that is, stationary gas phase).

Excellent absolute verification of the theory was obtained in an experimental study of rivulet flow on an inclined glass plate. All constants used were derived from theory. The flow rates studied varied from 0.03 to 260 cc./min. with rivulet widths varying from 2 to 50 mm. Plates angles of 10, 45, and 80 deg. were used. Water, glycerol-water mixtures (10 centipoise viscosity), and *n*-dodecane (25 dynes/cm. surface tension) were used to study physical property effects. Contact angles ranged from 3 to 16 deg., depending on surface conditions. In all cases of ripple-free flow the rivulet width was predicted by the theory to within about ± 20%.

At high liquid flow rates regular ripples appeared on the rivulets. The transition to ripple flow occurs at a Reynolds number of about 5 to 10. Very rough doubling of the width predicted from the ripple-free theory corresponds to the experimental results found under rippling conditions. Addition of surface-active agents suppresses the ripples and then very close agreement was again obtained with the theory.

ACKNOWLEDGMENT

The authors acknowledge the helpful theoretical suggestions of C. V. Sternling and the experimental assistance of J. L. Ralph.

NOTATION

a = $\sqrt{\gamma/\rho g \sin \alpha}$
b = constant, the radius of curvature at the stream centerline
$E(k, \phi)$ = elliptic integral of second kind
E = complete elliptic integral of second kind = $E(k, \pi/2)$
$F(k, \phi)$ = elliptic integral of first kind
g = acceleration due to gravity
K = complete elliptic integral of first kind = $F(k, \pi/2)$
k = $2/\sqrt{4 + \delta^2}$
l = stream width
N_{Re} = Reynolds number
P = dimensionless stream width = l/a = $l\left(\frac{\rho g \sin \alpha}{\gamma}\right)^{1/2}$
p = pressure
p_g = gas pressure
Q = volumetric flow rate
u = velocity component parallel to x axis, also Z/δ
v = velocity component parallel to y axis
w = velocity component parallel to z axis
X = x/a
x = coordinate parallel to plate and perpendicular to flow direction
Y = $(\eta_o - \eta)/a$
Y_o = Y at $X = 0$
y = coordinate perpendicular to plate and perpendicular to flow direction
Z = $Y + \delta$
z = coordinate parallel to flow direction

Greek Letters

α = angle of inclination between plate and vertical
β = angle in Figure 3
γ = liquid-vapor interfacial tension
δ = a/b
η = value of y at interface
η_o = η at $x = 0$
θ = contact angle
μ = viscosity of liquid
ν = μ/ρ
ξ = y/a
ρ = density of liquid
τ_{xy} = shear stress component
τ_n = normal stress
ϕ = variable as defined by Equation (34)
Ω = dimensionless flow rate = $\frac{\mu\rho g Q}{\gamma^2} \tan \alpha \sin \alpha$
ω = dimensionless velocity = $\frac{\mu w \tan \alpha}{\gamma}$

LITERATURE CITED

1. Goodrich, F. C., *Proc. Roy. Soc. (London)*, **A260**, 184 (1961).
2. von Karman, T., and M. A. Biot, "Mathematic Methods in Science and Engineering," McGraw-Hill, New York (1940).
3. King, L. V., "On the Direct Numerical Calculation of Elliptic Integrals," Cambridge Univ. Press (1924).
4. Langmuir, I., *J. Am. Chem. Soc.*, **59**, 2405 (1937).
5. Rayleigh, *Proc. Roy. Soc. (London)*, **A92**, 184 (1915).
6. Rayleigh, *Phil. Mag.*, **34**, 309 (1892).

Manuscript received January 3, 1966; revision received July 7, 1966; paper accepted July 7, 1966.